Integrated compact optical current sensors with high sensitivity

Duanni Huang*[a], Paolo Pintus[a,b], Sudharsanan Srinivasan[a], John E. Bowers[a]

a. Electrical and Computer Engineering Department, University of California Santa Barbara,
California 93106, USA;
b. Scuola Superiore Sant'Anna, via Moruzzi 1, 56124 Pisa, Italy

*duanni@umail.ucsb.edu

ABSTRACT

We demonstrate a Sagnac based fiber optic current sensor using only 10cm of terbium doped fiber with a high Verdet constant of 15.5 rad/Tm at a wavelength of 1300nm. Measurements of the fiber inside a solenoid show over 40dB of open loop dynamic range as well as a minimum detectable current of 0.1mA. In order to decrease size while increasing sensitivity even further, we consider integrated magneto-optic waveguides as the sensing element. Using silicon waveguides alongside magneto-optic material such as cerium doped yttrium iron garnet (Ce:YiG), we model the Verdet constant to be as high as 10,000 rad/Tm. This improvement by three orders of magnitude shows potential for magneto-optic waveguides to be used in ultra-high sensitivity optical magnetometers and current sensors. Finally, we propose a fully integrated optical current sensor using heterogeneous integration for silicon photonics.

Keywords: current sensors, fiber optic sensor, Faraday rotation, heterogeneous integration, silicon photonics

1. INTRODUCTION

Optical current sensors (OCS) offer several advantages when compared to Hall Effect and other conventional current sensors. These advantages include resistance to electromagnetic interference, suppression of spurious magnetic fields, and the placement of supporting electronic equipment away from the dangerous high voltage environment that often surround the sensor [1]. Due to the operating principle of fiber optic current sensors (FOCS), they are only sensitive to the magnetic fields that are produced by the current carrying wire, and insensitive to background fields such as Earth's magnetic field. Furthermore, FOCS generally have no conductive materials and are able to sense currents up to hundreds of kA with negligible saturation effects [2]. As a result, fiber optic current sensors have been used in electrowinning, power grids and other industries involving strong currents for many years.

More recently, emerging applications such as electric automobiles call for sensors with higher sensitivities and reduced footprint, while maintaining the inherent advantages of OCS. These applications often require sensitivities in the mA range while preserving a small footprint. Such metrics have not been achieved with current FOCS technology, which revolves around the use of silica fiber. In this paper, we explore several approaches that will increase OCS sensitivity and reduce footprint of the sensor. First, we use terbium doping of the fiber to increase sensitivity over twentyfold. A further improvement in sensitivity as well as a significant reduction in footprint can be achieved by using integrated waveguides as sensors instead of fiber. Finally, we examine the benefits of using heterogeneous integration with silicon photonics to fabricate an integrated "front-end" to drive the OCS instead of discrete components. Such an approach can greatly decrease the size, weight, cost, and power consumption of the sensor.

2. TERBIUM DOPED FIBER OPTICAL CURRENT SENSOR

2.1 Overview

The operating principle of a fiber optic current sensor is based on Faraday rotation. When linearly polarized light travels through a magnetic medium with a magnetic field applied parallel to the optical propagation direction, the light will undergo polarization rotation. Equivalently, when oppositely handed circularly polarized light passes through the medium, the two polarizations of light will travel at different speeds, which induces a relative phase shift between them.

This effect is nonreciprocal, in that it depends on whether the light is propagating with or against the magnetic field. The amount of Faraday rotation (θ_f) is dependent on the length of path interaction (l) between the light and the magnetic field (B), as well as a material parameter known as the Verdet constant (V) of the medium.

$$\theta_f = V \int_l \vec{B} \cdot \vec{dl} \tag{1}$$

Generally, the fiber will be orientated in such a way that it is exactly parallel with the magnetic fields produced by the current carrying wire. In this case, the expression above can be simplified to $\theta_f = VBl$. From this expression, it is clear that the sensitivity of the sensor is dependent on the Vl product. However, increasing the length of the fiber increases footprint and leads to significant linear birefringence within the fiber, which considerably dampens the measured signal. Standard silica fibers have a low Verdet constant (0.8 rad/T*m at 1300nm), which limit their use for high sensitivity OCS [3]. Terbium (Tb) doping of fiber has been shown to significantly increase the Verdet constant, up to a record 32rad/T*m that was measured at 1060nm [4]. A very short piece of Tb-doped fiber was used as a magnetic field sensor using polarimetric detection [5]. In the following sections, we also use Tb-doped fiber provided by Advalue Photonics in a similar polarimetric, as well as a Sagnac-based interferometric configuration for current and magnetic field sensing [6].

2.2 Polarimetric Sensor

The testing configuration for the polarimetric sensor is shown in Figure 1 below. Polarimetric detection, also known as direct detection, measures the polarization rotation as it passes through the sensing fiber due to the Faraday effect. Our testbed for the sensor is shown in Figure 1b. Instead of wrapping the Tb-fiber around a current carrying wire, we use a straight fiber inside a solenoid in order to simulate higher currents. Here, the Faraday rotation is given by $\theta_f = VNI$ where I is the current in the solenoid and N is the number of turns. We calculate N = 507 for the solenoid depicted, assuming uniform turn density. For 1A of DC current through the solenoid, we measure 6.5mT of B-field through an independent gaussmeter measurement. We use 10cm of Tb-doped fiber as the sensing element.
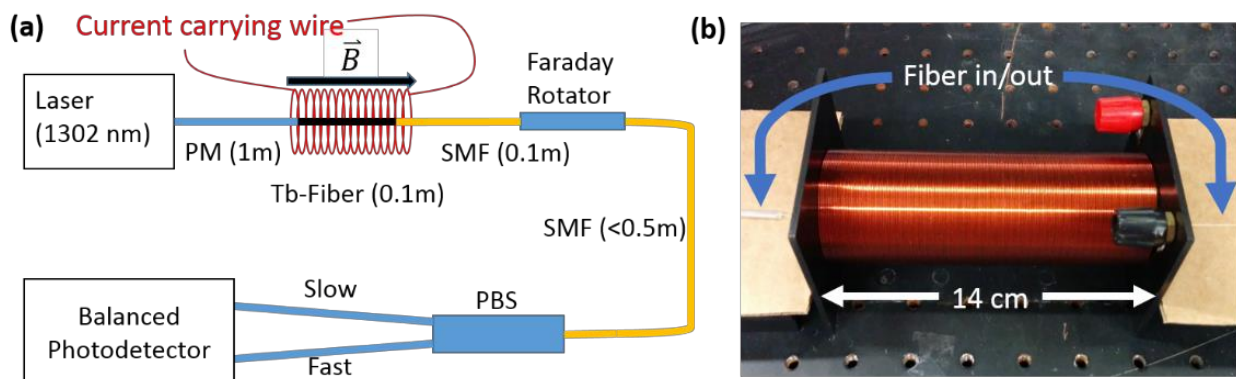
Figure 1. (a) Schematic of the polarization detection scheme. The sensor consists of a laser, the Tb fiber chain, a Faraday rotator, an in-line polarization beam splitter (PBS), as well as a balanced photodetector. (b) Picture of the 14cm long, 507 turn solenoid coil used to produce the magnetic field.

It is desirable to operate the sensor within telecom O (1260-1360nm) or C (1530-1565nm) bands due to wide availability of light sources and other optical components. At 1300nm, the total loss of the Tb fiber chain is measured to be 2.3dB. After subtracting 1.5dB of estimated loss from the two splices due to mode mismatch between the Tb fiber and PM or SMF (measured by Advalue Photonics at 1060nm), we obtain a propagation loss of 0.08 dB/cm at 1300nm. At 1550nm, the loss is considerably higher at 1.7dB/cm, and the Verdet constant is expected to be smaller at longer wavelengths. The light propagates through the Tb fiber chain, and through an in-line Faraday rotator that provides 45 degrees of polarization shift. Finally, the light passes through an in-line polarization beam splitter, and the intensity difference between the fast and slow axes is measured with a balanced detector. The total length of SMF in the sensor is kept short to minimize sensor size as well as polarization drift.

The intensities of each arm at the detector can be expressed as $P_{slow} = P_0 \cos^2(\theta + \theta_f)$ and $P_{fast} = P_0 \sin^2(\theta + \theta_f)$ where P_0 is the incident light power at the PBS and θ is the 45 degree polarization shift from the Faraday rotator. The normalized signal at the detector can be written as the following, for small Faraday rotation.

$$P_{BD} = \frac{P_0 \cos^2(\theta + \theta_f) - P_0 \sin^2(\theta + \theta_f)}{P_0 \cos^2(\theta + \theta_f) + P_0 \sin^2(\theta + \theta_f)} = \cos(2(\theta + \theta_f)) \tag{2}$$

$$P_{BD} = \cos(2\theta)\cos(2\theta_f) - \sin(2\theta)\sin(2\theta_f) \approx -(2\theta_f) \tag{3}$$

Thus, we expect a linear relation between the power at the detector and the applied current. Furthermore, the slope of the data is $-2VN$, and the Verdet constant of the fiber at 1300nm can be extracted. The figure below shows the detected powers as the DC current through the solenoid is swept from -1A to 1A and back over five minutes.
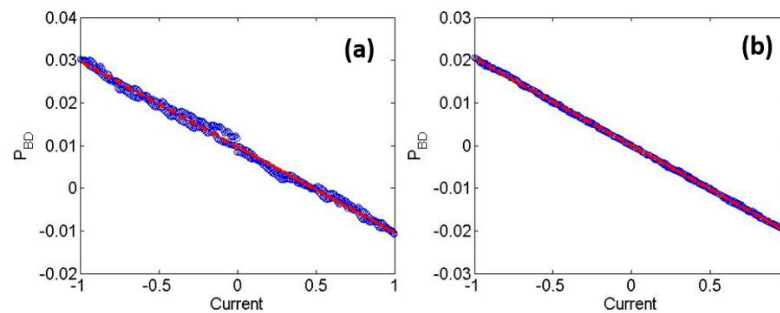
Figure 2. (a) The signal measured at the balanced detector as the current in the solenoid is swept from -1A to 1A (b) The output after calibration is done to cancel out any polarization drift in the system.

While the amount of polarization drift from the SMF and the Faraday rotator in the system is small, we can calibrate for it, as shown in Figure 2b to improve the linearity of the system. From this data, the calculated Verdet constant of the Tb-fiber at 1300nm is 15.5 rad/Tm, or 19.5 µrad/A. This is lower than the previously reported 32 rad/Tm at 1060nm, but expected due to the wavelength dependence of the Verdet constant.

2.3 Interferometric Sensor

While the direct, polarimetric detection is simple and useful for extracting the Verdet constant, it is not practical due to the random polarization drift in the system. For this reason, FOCS generally use an interferometric scheme using a Sagnac-loop interferometer [7,8]. This architecture has been studied extensively, and also used in high sensitivity fiber-optic gyroscopes [9]. The key difference here is that we detect the relative phase shift for counter-propagating circular polarizations rather than polarization rotation of linear polarization. This configuration is shown below in Figure 3.
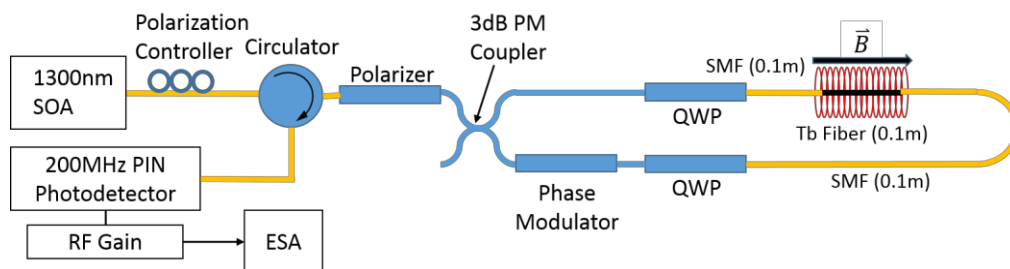
Figure 3. Schematic of the interferometric Sagnac-loop current sensor.

A semiconductor optical amplifier (SOA) pumps 4mW of amplified spontaneous emission (ASE) centered at 1300nm into the sensor. This is preferable to a laser due to the low optical coherence of the ASE, which reduces noise from

backscattering within a coherence length from the center of the Sagnac loop. The measured RIN of this source is -130dB/Hz. The light is polarized, and split into two paths through the 3dB coupler. Within the Sagnac loop, the linear polarization of light is transformed to circular polarization using quarter wave rotator (QWP) from Fibercore. The two circularly polarized waves then pass through the Tb fiber chain, where they undergo the nonreciprocal phase shift caused by the applied current. A lithium niobate modulator is used to modulate the phases of the counter-propagating light waves with an amplitude of 1.8 radians. The modulation frequency is 15.1 MHz, as governed by the loop length (6.8m). The nonreciprocal phase shift can be detected by interference at the 3dB coupler, and measured using a photodetector with subsequent RF gain with a combined responsivity of 5300V/W. The total detected optical power at the photodetector is 80μW. Finally, the signal is analyzed with an electrical spectrum analyzer, and the Faraday signal at the first harmonic of the modulation frequency is shown below.
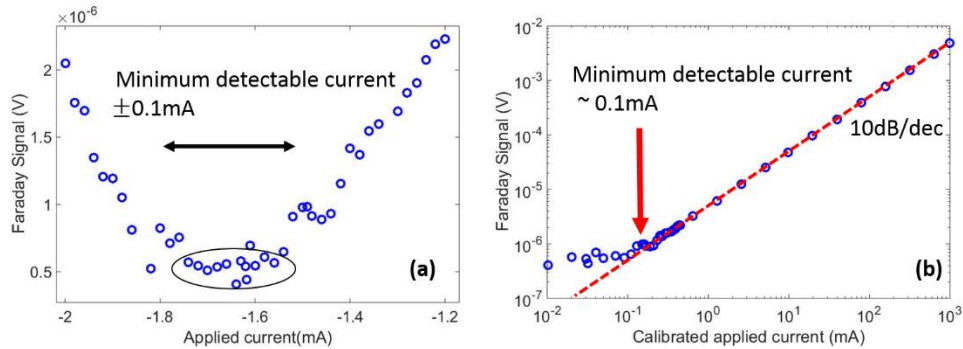
Figure 4. (a) The Faraday signal after applying RF gain. Measurements show that there is an offset of roughly -1.65mA in the system. (b) The Faraday signal measured over a much wider range of currents, after correcting the -1.65mA offset. Measurements exactly follow the predicted 10dB/dec slope until the applied current is ~0.1mA, which is the minimum detactable current for the system.

We sweep the applied current from -1A to 1A, and zoom in on the region of interest where the Faraday signal is at a minimum, as depicted in Fig. 4(a). The minimum of the Faraday signal occurs at -1.65mA. This is not zero because we pick up Earth's magnetic field in this measurement. If the fiber was instead looped around a current carrying wire, there would be no signal from background fields due to the optical path. There is a 0.1mA window on either side of the minimum point for which there is no change in the Faraday signal, as illustrated by the oval. This suggests that the sensor cannot accurately detect currents in that range. This is better depicted in Fig. 4(b), in which we clearly observe a rolloff in the slope for an applied current below the minimum detectable current of 0.1mA. The dynamic range of the system in this open-loop configuration is over 40dB and can be improved further with feedback techniques or serrodyne modulation [10].

The Verdet constant of the fiber can also be extracted from Fig. 4. Due to the sinusoidal modulation of the phase modulator, the Faraday signal is given by the following.

$$V_{Faraday}(\theta_f) = P_0 \eta J_1(1.8)\sin(2\theta_f) \qquad (4)$$

Here, P_0 is the 80μW of detected optical power, η is the 5300V/W total responsivity, and $J_1(1.8)$ is the Bessel function of the first order at its maximum modulation amplitude of 1.8 radians. Once again assuming small angle approximation, we calculate the Verdet constant to be 15.3 rad/Tm. This is in excellent agreement with the results from the polarimetric sensor. Since the Faraday rotation will increase with longer fiber length, we can extrapolate our results for longer Tb fiber. For this extrapolation, we assume a practical setup in which the Tb doped fiber is wrapped around a straight current carrying wire. As the diagram shows in Fig. 5(a), our measured data for a N=507 solenoid can be carried over into an equivalent setup with 507 turns of 10cm circumference fiber. From here, we calculate the sensitivity for a single loop of fiber, and then extrapolate for longer lengths. The limiting factor is the 0.08dB/cm propagation loss of the Tb fiber, which is modelled in Fig. 5(b), assuming the same noise floor for our system.
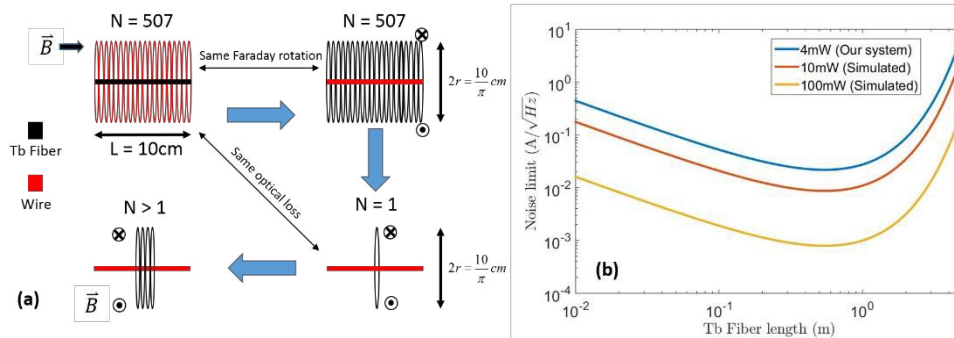
Figure 5. (a) Conversion from our experimental setup (top left) to a more practical current sensing setup with a straight wire and loops of fiber (top right). To keep the same optical loss, we keep the same length of fiber (bottom right). Now, we can extrapolate the results to multiple loops of fiber (bottom left). (b) Extrapolation of FOCS performance vs length of Tb fiber given our system noise floor and measured propagation loss for various ASE output powers.

The optimal length is for 0.5m of Tb fiber, for which the noise limit is 22mA/√Hz. For even longer fibers, the exponential decrease of received optical power dominates over the linear increase in sensitivity. If the loss in Tb fiber can be reduced or the incident power is increased, then the noise limit can be pushed further down. Finally, an alternate configuration [11] using an in-line reflection based interferometer can demonstrate a higher sensitivity by a factor of two, and will be a topic of exploration in the future.

3. CERIUM SUBSTITUTED YTTRIUM IRON GARNET WAVEGUIDE SENSOR

Another, more significant increase of sensitivity is potentially possible by moving away from fiber optics. Many materials show very high Faraday rotation, but few show both high Faraday rotation as well as low optical loss. Cerium substituted yttrium iron garnet (Ce:YIG) is an interesting exception, and has already seen use in isolator and circulator devices for integrated photonics, and has been proposed for use as a magnetometer [12]. While optical loss in Ce:YIG (~60dB/cm) is much larger than that of fiber, its Faraday rotation is also much higher, and reaches nearly 8000 radians/meter when the magnetization is saturated [13].

The operating principle behind a waveguide sensor is slightly different than that of a fiber sensor. Instead of detecting the magnetic field that is parallel to the sensor, it is necessary to detect fields that are perpendicular instead. This partially arises from the fact that almost all waveguides are highly birefringent, and thus it is difficult to obtain circular polarization. Instead, by applying a magnetic field perpendicular to the waveguide in the following geometries, we can also achieve a nonreciprocal phase shift, depending on the polarization of the light (TE or TM).

Figure 6. (left) The waveguide geometry required for magnetic field induced nonreciprocal phase shift for transverse electric (TE) modes. (right). The waveguide configuration required for TM modes.

Also, the effective Verdet constant of the material depends on the polarization of the light. For the TE mode geometry (left), the magnetic field must be out of plane with respect to the waveguide. In this configuration, the saturation field of Ce:YIG is around 0.2T. For the TM mode geometry (right), the magnetic field must be in the same plane as the waveguide. In this configuration, the saturation field of Ce:YIG is much smaller, around 0.0005T [14]. The amount of nonreciprocal phase shift for each configuration is dependent on the exact dimensions of the waveguide, as well as the materials involved. For this calculation, we assume a silicon core waveguide with silica cladding, although we could easily use a low-loss silicon nitride core instead. Given a particular waveguide geometry, we then utilize finite element method to calculate the forward and backward propagating modes, and extract the nonreciprocal phase shift [15, 16]. From this we calculate that

the effective Verdet constant for TE modes is nearly 10,000 rad/Tm, while it is closer to 1,000,000 rad/Tm for TM modes. We note that a sensor operating in the TM mode may not be as useful due to the low saturation value of the magnetization. Once the Ce:YIG is saturated, then we no longer see a linear relation between the nonreciprocal phase shift and the applied magnetic field. Nevertheless, the Verdet constants here are orders of magnitude higher than that found in Tb-fiber.

One potential disadvantage of a waveguide sensor when compared to FOCS is its lack of suppression of spurious magnetic fields. Since the sensor is sensitive to all fields that are perpendicular to the waveguide, it will pick up background fields from Earth's magnetic field, as well as local sources of magnetic field from nearby electronic equipment. However, this can be overcome by using two sensors in a differential configuration on each side of a current carrying wire. Background fields will be common to both sensors, and can be cancelled out.

4. HETEROGENEOUS INTEGRATION

Regardless of whether the Tb-doped fiber sensor or a Ce:YIG waveguide sensor is more attractive, it is possible to utilize heterogeneous integration for silicon photonics to fabricate a "front-end" photonic integrated circuit (PIC) for the Sagnac loop. Wafer bonding is key in heterogeneous integration in that it allows us to circumvent lattice mismatch between the silicon substrate and the epitaxial layer, which is a major limitation to monolithic approaches. For example, III-V materials are bonded onto silicon on insulator (SOI) substrates and subsequently processed to form lasers and other light sources on chip [17,18]. This is significant since silicon is not an efficient light emitter due to its indirect bandgap. Furthermore, the same process can be used to bond Ce:YIG for use as the integrated waveguide sensor.

Heterogeneous integration on silicon allows to utilize a flexible platform to design PICs for. As previously shown in Figure 3 as well as below, the front-end of the Sagnac-based sensor requires multiple photonic components. In addition to a source to drive the sensor, this PIC also requires photodiodes and modulators. The choice of light source is an interesting topic. Traditionally, interferometric based sensors use light emitting diodes (LED) or ASE sources due to their incoherent nature. If a coherent source such as a laser is used instead, the sensor is negatively affected by coherent reflections from backscattering points in the Sagnac loop. These reflections can interfere with the primary signal. Thus, ASE sources are the preferred device in optical gyroscopes and other interferometric sensors. However, heterogeneous silicon lasers have larger output power as well as lower RIN than ASE sources on chip. For this reason, it is preferable to use lasers on an integrated platform. To suppress the coherent noise, we are investigating an approach in which we apply frequency modulation to the laser [19]. The resulting effect is a broadening of the laser linewidth, which destroys the coherence of the device. This allows us to retain the high power and low RIN of a laser, while not suffering too much from coherent backscattering within the loop.
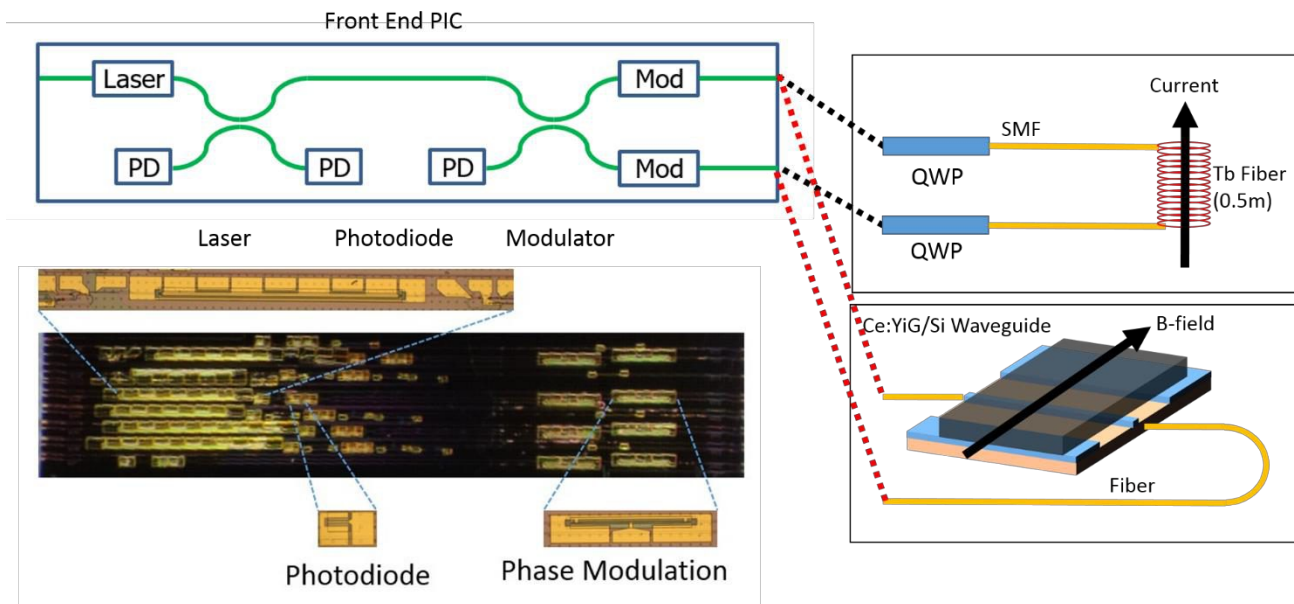
Figure 7. (left) The front end PIC for a Sagnac-based sensor is fabricated using heterogeneous integration on silicon. The front-end can be packaged with a Tb-fiber current sensor (top right) as well as a Ce:YIG waveguide sensor (bottom right).

We fabricated this chip with over twenty different configurations of the Sagnac front-end PIC. These configurations included splits on laser geometry, photodiode area, as well as various splits on the modulator. The PIC can be tested with both the Tb-fiber sensor, as well as a Ce:YIG waveguide sensor. A pair of quarter wave rotators are required for use with the fiber sensor, as the polarization needs to be circular. No polarization rotation is needed for use with the waveguide sensor. We are currently testing the performance of the front-end PIC, which can be packaged and used with any Sagnac based sensor, including integrated optical gyroscopes if successful [20]. The total area of the PIC is less than 0.1cm^2.

5. CONCLUSIONS

In conclusion, we have shown the feasibility of using terbium-doped fiber with a high Verdet constant of 15.5 rad/Tm as the sensing element in a compact, highly sensitive current sensor. We are able to sense DC currents down to 0.1mA using a test setup with a 507 turn solenoid. Finally, we extrapolate our measurements to find a noise limit of 22mA/√Hz for a practical Tb fiber current senor with a length of just 0.5 meter. This sensor shows promise for high sensitivity applications in which it is not possible to use tens or hundreds of meters of fiber. Further improvements to this technology can be made by spinning the Tb fiber and decreasing the propagation loss. We have also proposed using Ce:YIG as the sensing element in a magneto-optic waveguide sensor. Our simulations show a Verdet constant near 10,000 rad/Tm, which could lead to ultra-high sensitivity optical current sensors and optical magnetometers. Finally, we are exploring the use of heterogeneous integration of silicon photonics to create highly functional, highly compact PICs to be used with the Sagnac architecture. This can be used with both fiber sensors as well as waveguide sensors, reducing the overall size and power consumption.

ACKNOWLEDGMENTS

REFERENCES

[1] R. M. Silva, H. Martins, I. Nascimento, J. M. Baptista, A. L. Ribeiro, J. L. Santos, P. Jorge, and O. Frazão, "Optical current sensors for high power systems: a review," Appl. Sci. **2**(3), 602-628 (2012).

[2] K. Bohnert, P. Gabus, H. Brändle, and P. Guggenbach. "Fiber-optic dc current sensor for the electro-winning industry," Proc. SPIE **5855**, 210-213 (2005).

[3] J. Noda, T. Hosaka, Y. Sasaki, and R. Ulrich. "Dispersion of Verdet constant in stress-birefringent silica fibre," Electron. Lett. **20**(22), 906-908 (1984).

[4] L. Sun, S. Jiang, and J. R. Marciante. "Compact all-fiber optical Faraday components using 65-wt%-terbium–doped fiber with a record Verdet constant of 32 rad/(Tm)," Opt. Express **18**(12), 12191-12196 (2010).

[5] L. Sun, S. Jiang, and J. R. Marciante. "All-fiber optical magnetic-field sensor based on Faraday rotation in highly terbium-doped fiber," Opt. Express **18**(6), 5407-5412 (2010).

[6] K. Bohnert, P. Gabus, J. Nehring, and H. Brandle. "Temperature and vibration insensitive fiber-optic current sensor," J. Lightwave Technol. **20**(2), 267 (2002).

[7] D. Huang, S. Srinivasan, and J. E. Bowers, "Compact Tb doped fiber optic current sensor with high sensitivity," Opt. Express **23**(23), 29993-29999 (2015).

[8] P. A. Nicati, and P. Robert. "Stabilised current sensor using Sagnac interferometer," J. Phys. E. Sci. Instrum. **21**(8), 791 (1988).

[9] H. C. Lefevre, *The Fiber-optic Gyroscope* (Artech house, 1993).

[10] C. J. Kay, "Serrodyne modulator in a fibre-optic gyroscope," in *IEE Proceedings J. Optoelectronics*, **132**(5), (IET, 1985) pp. 259-264.

[11] G. Frosio, and R. Dändliker. "Reciprocal reflection interferometer for a fiber-optic Faraday current sensor," Appl. Opt. **33**(25), 6111-6122 (1994).

[12] S. Srinivasan, and J. E. Bowers. "Integrated High Sensitivity Hybrid Silicon Magnetometer," IEEE Photon. Technol. Lett. **26**(13), 1321 (2014).

[13] B. Stadler and T. Mizumoto, "Integrated magneto-optical materials and isolators: a review." IEEE Photon. J.**6**(1), 1-15 (2014).

[14] T. Goto, M. Onbaşil, and C. A. Ross. "Magneto-optical properties of cerium substituted yttrium iron garnet films with reduced thermal budget for monolithic photonic integrated circuits," Opt. Express **20**(27), 28507-28517 (2012).

[15] P. Pintus, "Accurate vectorial finite element mode solver for magneto-optic and anisotropic waveguides," Opt. Express **22**(13), 15737-15756 (2014).

[16] P. Pintus, D. Huang, S. Srinivasan, and J. E. Bowers. "Full vectorial mode solver for design and optimization of magneto-optic devices," in Electromagnetics in Advanced Applications (ICEAA), (2015).

[17] T. Komljenovic, et al. "Heterogeneous Silicon Photonic Integrated Circuits." (2015).

[18] M. J. Heck, J. F. Bauters, M. L. Davenport, J. K. Doylend, S. Jain, G. Kurczveil, S. Srinivasan, Y. Tang, and J. E. Bowers. "Hybrid silicon photonic integrated circuit technology," IEEE J. Sel. Topics Quantum Electron. **19**(4), (2013).

[19] Y. Shen, M. Tran, S. Srinivasan, J. Hulme, J. Peters, M. Belt, S. Gundavarapu, Y. Li, D. Blumenthal, and J.E. Bowers. "Frequency modulated laser optical gyroscope," in International Photonics Conference (IPC), (2015).

[20] S. Srinivasan, R. Moreira, D. Blumenthal, and J. E. Bowers. "Design of integrated hybrid silicon waveguide optical gyroscope," Opt. Express **22**(21), 24988-24993 (2014).